Available online at www.sciencedirect.com
SCIENCE DIRECT®
Journal of Nuclear Materials 348 (2006) 60–69
journal of nuclear materials
www.elsevier.com/locate/jnucmat

Sorption of silicon on magnetite and other corrosion products of iron

Violaine Philippini [a], Aude Naveau [b], Hubert Catalette [a,*], Stéphanie Leclercq [a]

[a] Electricité de France, Research and Development, Les Renardières, Route de Sens-Ecuelles, 77 818 Moret sur Loing cedex, France
[b] Université de Reims, GRECI, Chimie de Coordination des Interfaces, BP 1039, 51687 Reims cedex 2, France

Received 4 July 2005; accepted 6 September 2005

Abstract

The sorption of Si on various iron corrosion products of nuclear waste canisters (magnetite Fe_3O_4, goethite α-FeOOH, and siderite $FeCO_3$) and pyrite FeS_2 was evidenced in the presence of a background electrolyte (NaCl or $NaClO_4$). For magnetite, goethite and siderite, Si sorption increased with pH in the 3–7 pH range. It reached a plateau, and finally it decreased at pH more than 9. Sorption capacities were determined for magnetite (19×10^{-6} mol_{Si} $g^{-1}_{magnetite}$), goethite (79×10^{-6} mol_{Si} $g^{-1}_{goethite}$) and siderite (20×10^{-6} mol_{Si} $g^{-1}_{siderite}$), while it could be neglected for pyrite since it is almost zero. Sorption data on magnetite was modelled using a surface complexation model with the bidentate surface complex $(\equiv XO)_2Si(OH)_2$ and $\log K_{complexation} = 8.6$. Influence of magnetite on glass lifetime was evaluated and it was estimated negligible.

PACS: 28.41.Kw

1. Introduction

When high level radioactive wastes (HLRW) are vitrified, the glasses are teemed into stainless steel containers, and they will be put in black steel overpacks, which need to have a sufficiently long lifetime, namely 1000 years. It should prevent contact of glass with water at high temperatures (90–150 °C) during the nearly complete radioactive decay of the short live radionuclides. These waste packages could be disposed into a steel cased tunnel in an eventual geological repository [1]. For these packages, the casing lifetime should be controlled by their corrosion behavior. The canister is supposed to be corroded due to the presence of groundwater [2]. Thus, nuclear glasses could be in contact with corrosion products such as magnetite (Fe_3O_4), goethite (α-FeOOH), siderite ($FeCO_3$) and pyrite (FeS_2) which is naturally present in the clayed host rock [3,4].

Glass alteration is a complex phenomenon which depends on intrinsic glass properties (composition, structure, surface ...) and its environment (temperature, pH, aqueous solution composition ...). The basic mechanisms of glass alteration can be divided into three parts [5].

* Corresponding author. Tel.: +33 (1) 60 73 78 67; fax: +33 (1) 60 73 68 89.
E-mail address: hubert.catalette@edf.fr (H. Catalette).

0022-3115/$ - see front matter © 2005 Elsevier B.V. All rights reserved.
doi:10.1016/j.jnucmat.2005.09.002

- When water comes in contact with glass, it diffuses into the pristine glass, and exchanges its protons with the most mobile ions (Na^+, Li^+, Cs^+, Ca^{2+}, Sr^+ ...). The glass network then undergoes a congruent dissolution. During this phase, glass dissolves at its initial rate.
- Under static leaching conditions, typical of a geological repository, this phase is followed by an intermediate phase during which the alteration rate decreases. Indeed, glass alteration is expected to be limited by in situ recondensation of a fraction of hydrolyzed elements (Si, Al, Zr, Ca ...), which can lead to the formation of an amorphous alteration layer (or gel). This gel can act as a diffusion barrier. It can only form in saturation conditions, i.e. when the leaching solution is saturated with silicon. For this reason it is important to predict whether Si sorption on corrosion products could occur in undersaturation conditions.
- Finally, the alteration is governed by the residual rate, four orders of magnitude lower than the initial rate.

Since glass and corrosion products may be in contact, the uptake of silicon by corrosion products is possible. Achieving the saturation conditions would be delayed, which could limit the protective properties of the altered layer. Sorption of silicon onto magnetite, goethite, siderite and pyrite surfaces could therefore speed up glass alteration. Studying sorption processes is fundamental for assessing the glass lifetime in deep geological disposal. As a consequence, understanding the retention properties of each corrosion product is necessary. Jollivet et al. [6] carried out tests on non-radioactive French nuclear glass in the presence of simulated metal canister corrosion products. They showed that the glass alteration process varied in the presence of corrosion products, but it can be argued that they did not use representative corrosion products.

The aim of the present study is to estimate the uptake of Si by corrosion products (to better understand the reactivity of the corrosion products in contact with aqueous solutions containing silicon species), and to predict the glass alteration. The diffuse layer model, a surface complexation model, is currently used to interpret sorption experimental data. It is implemented in the FITEQL code [7], which can also fit the surface binding properties of magnetite by deriving the surface complexation constants. In addition, the geochemical JCHESS code [8] was used to take into account the aqueous speciation of silicon. The aim of this theoretical approach is to predict the sorption of silicon species on corrosion product surfaces, and to better understand the surface reactions occurring when corrosion products and glass are present simultaneously in water.

2. Experimental details

2.1. Materials

Magnetite, goethite and pyrite characterizations have been previously observed [9–11], and siderite was synthesized by Musy et al. from the Commissariat à l'Energie Atomique (C. Musy, C. Bataillon, P. Vigier, D. Besnard and A. Chénière, unpublished results). Musy et al. aimed to synthesize corrosion products of iron by oxidizing powdery iron at 90 °C. Iron was introduced into a carbonated solution containing a small quantity of calcium. They studied the corrosion products formed in aerobic and anaerobic conditions.

Magnetite from Alfa, was characterized by Mössbauer spectrometry and by X-ray diffraction (XRD). It was found to be almost a pure magnetite phase slightly oxidized to hematite. Scanning Electron Microscopy (SEM) showed grains whose size was about 500 nm, which agglomerate into 33 μm aggregates. The specific surface area ($1.8 \pm 0.2\ m^2\ g^{-1}$) was measured by the classical Brunauer–Elmet–Teller method using a multiple point adsorption nitrogen process (BET-N_2).

Goethite from BASF, was characterized by Mössbauer spectrometry, and by XRD. It was found to be a pure goethite phase. SEM showed grains of different sizes (0.2 μm, 1 μm, 2 μm) agglomerated as 20 μm aggregates. The specific surface area ($20 \pm 2\ m^2\ g^{-1}$) was measured by the method we also used for magnetite. Finally, chemical analysis by the Particle Induced X-ray Emission (PIXE) method showed the presence of sulfur (0.31 ppm), magnesium (0.11 ppm) and calcium (0.06 ppm).

Siderite was studied by XRD. It was found to be almost a pure siderite phase with a tiny amount of Fe metal. SEM showed some 10 μm aggregates. The specific surface area, measured by the BET-N_2 method, was found to be equal to $0.45 \pm 0.02\ m^2\ g^{-1}$.

Pyrite from Alfa Johnson Matthey, was characterized by Mössbauer spectrometry and by XRD. It was found to be almost a pure pyrite phase (small

amounts of pyrrhotite were detected by XRD). SEM showed grains, whose size was less than 50 μm. The specific surface area (0.80 ± 0.04 $m^2\,g^{-1}$) was, once more, measured by the BET-N_2 method. The solid was washed by a 10^{-2} mol L^{-1} nitric acid solution in a glove box under nitrogen atmosphere, and then washed with distilled water. Thanks to these experimental conditions, no oxidation product was detected by X-ray Photoelectron Spectroscopy (XPS) on the corrosion product surface.

Distilled (Milli-Q Academic System, Millipore) and outgassed (by bubbling argon) water was used in all experiments. The background electrolytes were Prolabo NaCl and $NaClO_4$ solutions (purity 99.5%). The silicon solution used was a 1000 ppm Titrisol commercial solution. All other chemicals were of reagent grade. They were stored in polypropylene flasks to avoid the possible contamination with silicon.

2.2. Potentiometric titrations

Prior to modelling sorption of ions on a solid surface using a surface complexation model, surface site densities have to be determined. A classical method to determine surface site density consists in using acid–base titrations. Assuming that surface sites ($\equiv$ XOH) are amphoteric, i.e., can be either protonated to form ($\equiv XOH_2^+$) or deprotonated to form ($\equiv XO^-$), results from acid–base titrations of the surface provide concentration of protonated and deprotonated sites, which can then lead to the sites density [12–15]. The reactions of protonation and deprotonation are:

$$\equiv XOH_2^+ \rightleftharpoons \equiv XOH + H^+ \quad K_{a1}, \tag{1}$$

$$\equiv XOH \rightleftharpoons \equiv XO^- + H^+ \quad K_{a2}, \tag{2}$$

where $\equiv$ XOH, $\equiv XOH_2^+$ and $\equiv XO^-$ represent neutral, positively charged, and negatively charged functional groups on the solid surface, and K_{a1} and K_{a2} are the intrinsic acidic constants.

Potentiometric titrations of aqueous suspensions of corrosion products (10 g L^{-1}) were carried out under Ar atmosphere with a Metrohm 665 titrator equipped with a combined electrode (glass electrode associated to a reference Ag/AgCl/NaCl 3 mol L^{-1} electrode). The electrode was calibrated in concentration using either 10^{-2} and 10^{-4} mol L^{-1} HCl solutions in NaCl at the same ionic strength as for batch experiments or pH buffer solutions from SCHOTT (pH = 4.01, 6.87 and 9.18). Suspensions of corrosion products in sodium chloride electrolyte were magnetically stirred during the measurements. Small aliquots (50 μL) of either base or acid (NaOH or HCl 0.1 mol L^{-1}) were added every 210 s.

2.3. Sorption experiments

Sorption studies were performed in batches. Twenty five or fifty milliliters aqueous solution of background electrolyte was added to 50–500 mg of corrosion product in polystyrene tubes. The pH was adjusted with 0.1 mol L^{-1} HCl or NaOH aqueous solutions, then the tubes were stirred with a wrist action shaker for 15 or 24 h. After stirring, suspensions were filtered through 0.20 μm cellulose acetate membranes. The pH of the filtrate was immediately measured, the total concentration of non-sorbed anions was determined by inductively coupled plasma-atomic emission spectroscopy (ICP-AES JY 38 S, Jobin Yvon). All experiments were carried out at room temperature. The quantity of silicon sorbed onto corrosion products was calculated by subtracting the remaining silicon aqueous concentration from the introduced silicon concentration.

3. Treatment of data

3.1. Sorption on magnetite

The results of sorption experiments were expressed as the percentage of adsorbed silicon vs pH. The experimental results for magnetite, which is the most representative corrosion product, were modelled to fit Si sorption on magnetite by using the FITEQL code. It includes a surface complexation model, the double-layer model. In this model, the oxide/solution interface is described as two charged layers. The first layer is made by the specifically adsorbed ions. The second one is a diffuse layer, that balances the surface charge. The distribution of ions in the latter follows the Gouy–Chapman formula. Mass action law equations corresponding to the protonation or the deprotonation of the surface sites are:

$$K_{a1} = \frac{[\equiv XOH]\{H^+\}}{[\equiv XOH_2^+]} \exp\left(\frac{F\Psi}{RT}\right), \tag{3}$$

$$K_{a2} = \frac{[\equiv XO^-]\{H^+\}}{[\equiv XOH]} \exp\left(\frac{F\Psi}{RT}\right), \tag{4}$$

where [] are the concentrations and {} the activities. The exponential represents the coulombic term that accounts for electrostatic effects [12]. F is the Faraday constant (C mol^{-1}), Ψ the surface potential (V), R the molar gas constant (J mol^{-1} K^{-1}) and T the absolute temperature (K). The value of Ψ is calculated by solving the Gouy–Chapman equation in a bulk aqueous solution containing a $z{:}z$ electrolyte:

$$\sinh\frac{ze\Psi}{2kT} = \frac{\sigma(8\epsilon_a\epsilon_0 kT)^{1/2}}{c^{1/2}}, \tag{5}$$

$$\sigma = \frac{\sqrt{c}}{(8\epsilon_a\epsilon_0 kT)^{1/2}}\sinh\frac{ze\Psi}{2kT} = 0.1174\sqrt{I}\sinh\frac{zF\Psi}{2RT}, \tag{6}$$

where e is the elementary charge (1.602×10^{-19} C), k the Boltzmann's constant (1.381×10^{-23} J K^{-1}), ϵ_0 the permittivity of free space (8.854×10^{-12} C^2 J^{-1} m^{-1}) and ϵ_a the dielectric constant of water (78.54), σ the surface charge density (C m^{-2}), c the number of ions per volume ($6.022\times10^{23}\times$(ion concentration in mol L^{-1})) and I the ionic strength (mol L^{-1}).

If H^+ is the only sorbing ion, the surface charge density (σ), is given by:

$$\sigma = \frac{F([\equiv XOH_2^+] - [\equiv XO^-])}{SA} = \frac{F(C_A - C_B - [H^+] - [OH^-])}{SA}, \tag{7}$$

where A is the specific surface area (m^2 g^{-1}), S the solid concentration (g L^{-1}), C_A and C_B are the molar concentration of the added acid or base (mol L^{-1}). The molar concentrations of H^+ and OH^- are calculated from pH measurements.

FITEQL optimizes the surface complexation constant by minimizing the differences between calculated and experimental data using a non-linear least square optimisation algorithm.

3.2. Saturation experiments

The saturation curves showed a nearly linear behavior up to the saturation of the sorption sites with a Langmuir-type behavior. The linear form of the Langmuir equation can be written as follows:

$$\frac{1}{\Gamma} = \frac{1}{\Gamma_{max}} + \frac{1}{\Gamma_{max}K_{ads}[Si]}, \tag{8}$$

where Γ is the amount of Si adsorbed (mol g^{-1}), [Si] is the silicon equilibrium concentration (mol L^{-1}), Γ_{max} is the limiting value for the monolayer capacity Γ (mol g^{-1}) and K_{ads} is the equilibrium constant of the sorption reaction (mol L^{-1}). The results of saturation experiments were expressed as the logarithm of the adsorbed silicon concentration vs the logarithm of the silicon concentration at the equilibrium. The experimental results were fitted with the Langmuir equation in order to determine the sorption capacity of each corrosion product.

4. Results and discussion

4.1. Determination of surface site density

The method used to determine hydration time consisted in performing series of titrations after different stirring times. Hydration equilibrium was considered achieved when titration curves remained unchanged with increasing stirring times [16]. Applying this method to a corrosion product/NaCl (or $NaClO_4$) solution system led to an equilibration time of 4 h for magnetite and goethite, which is faster than previously determined: 72 h for magnetite [9] and 24 h for goethite [11]. Sorption experiments for magnetite, goethite and siderite were therefore carried out with 15 h stirring times. However, the pyrite/$NaClO_4$ solution system did not achieve equilibration even after 4 days. This was certainly due to pyrite oxidation by dissolved O_2 [17]. Indeed, when experiments were carried out in a glove box under anoxic conditions ($O_2 < 1$ ppm), the system led to an equilibration time lower than 24 h. Nevertheless, the surface site density could not be determined due to the partial dissolution of the solid.

Potentiometric titration of 10 g L^{-1} magnetite suspensions in 0.1 mol L^{-1} sodium chloride solutions led to a site concentration of 2×10^{-5} mol g^{-1}, which corresponds to a site density of 6.7 sites nm^{-2}, based on a specific surface area of 1.8 m^2 g^{-1}.

Potentiometric titration of 10 g L^{-1} goethite suspensions in 0.1 mol L^{-1} sodium chloride solutions led to a site concentration of 5.7×10^{-5} mol g^{-1}, which corresponds to a site density of 1.3 sites nm^{-2}, based on a specific surface area of 20 m^2 g^{-1}.

Potentiometric titration of siderite could not be performed because of its poor stability: siderite dissolved in aqueous solutions for pH less than 5.5 or more than 10.5, Fe(II) oxidized into Fe(III) and new oxide/hydroxide phases precipitated. The total proton sites concentration could not be determined. All the determined properties of the solids are summarized in Table 1.

Table 1
Specific surface area and total proton sites of the corrosion products

	Specific surface area ($m^2\ g^{-1}$)	Total proton sites (mol g^{-1})
Magnetite	1.8 ± 0.2	2×10^{-5}
Goethite	20 ± 2	5.7×10^{-5}
Siderite	0.45 ± 0.02	Not determined
Pyrite	0.80 ± 0.04	Not determined

4.2. Sorption studies

The speciation of silicon was first calculated as a function of pH with the JChess code (Fig. 1). In our experimental conditions, i.e., 5×10^{-4} mol L^{-1} of amorphous silica, and 0.1 mol L^{-1} of sodium chloride, quartz is quite soluble: 1×10^{-4} mol L^{-1}. Neglecting polynuclear species, whose concentration is lower than 10^{-8} mol L^{-1}, three aqueous species of silicon are formed above pH 7: H_4SiO_4, $H_3SiO_4^-$ and $H_2SiO_4^{2-} \cdot H_4SiO_4$ is predominant below pH 9, $H_3SiO_4^-$ is predominant between pH 9 and pH 12 and $H_2SiO_4^{2-}$ is predominant above pH 12.

The effect of pH on silicon sorption was studied for each corrosion product for pH values ranging from 2 to 12. We first studied the maximal sorption capacity of each solid (the results are summarized in Table 2). Saturation experiments were carried out at the maximal pH of sorption. This pH value also corresponds to the expected pH during glass leaching in underground conditions (pH 8.5).

Taking all the uncertainties of the measuring equipment into account, we estimated a 10%-uncertainty on the sorption experimental results.

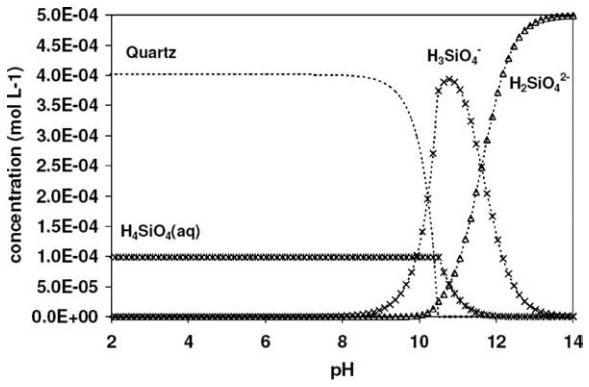

Fig. 1. Speciation curve of silicon calculated with the geochemical code JCHESS for a 5×10^{-4} mol L^{-1} amorphous silicon solution calculated from the thermodynamic data of Table 5. Only major species are shown.

Table 2
Sorption capacity of each corrosion product

	Sorption capacity ($\mu mol_{Si}\ g^{-1}$)
Magnetite	19 ± 14
Goethite	79 ± 21
Siderite	20 ± 8
Pyrite	No sorption

For magnetite, goethite and siderite, the graph that shows the effects of pH on the amount of Si sorbed can be divided into three parts (Fig. 2). The amount of Si sorbed first increases with pH in acidic conditions. In neutral to slightly alkaline conditions a plateau is reached, while in more alkaline conditions the quantity of Si uptaken decreases with pH.

For magnetite, goethite and siderite, the graph that shows saturation was fitted with the Langmuir equation in order to determine the sorption capacity of each corrosion product (Fig. 3). Langmuir equation does not take electrostatic effects into account, but they can be neglected at saturation.

4.2.1. Magnetite

Fig. 2 shows the effects of pH on the amount of Si sorbed (4.70×10^{-5} mol L^{-1} solution) on magnetite (2 g L^{-1}) in 0.1 mol L^{-1} NaCl electrolyte. The first part of the graph reveals a slow growth from 16.5% at pH 3.4 up to 22% at pH 7.6. The second part presents a plateau at 22% from pH 7.6 to pH 9.5. The third part shows a rapid decline from 22% at pH 9.5 down to 0% at pH 11.2. So, sorption curve leads to a maximal sorption onto magnetite surface from pH 7.6 to pH 9.5.

Saturation curve for suspension of different magnetite concentrations (from 0.5 to 50 g L^{-1}) in 0.1 mol L^{-1} sodium chloride with various concentrations in silicon (ranging from 25 to 500 μmol L^{-1}) at pH 8.5, leads to a sorption capacity of 19 ± 14 $\mu mol_{Si}\ g^{-1}_{magnetite}$ (Fig. 3).

4.2.2. Goethite

Fig. 2 shows the effects of pH on the amount of Si sorbed (10^{-4} mol L^{-1} solution) on goethite (1 g L^{-1}) in 0.1 mol L^{-1} NaCl electrolyte. The first part of the graph reveals a regular rise from 0% at pH 2.3 up to 100% at pH 7.9. Then, the line graph reaches a plateau from pH 7.9 to pH 9.7. The last portion shows a steep decrease from 100% at pH 9.7 down to 47% at pH 11.5. So, sorption curve leads to a maximal sorption onto goethite surface from pH 7.9 to pH 9.7.

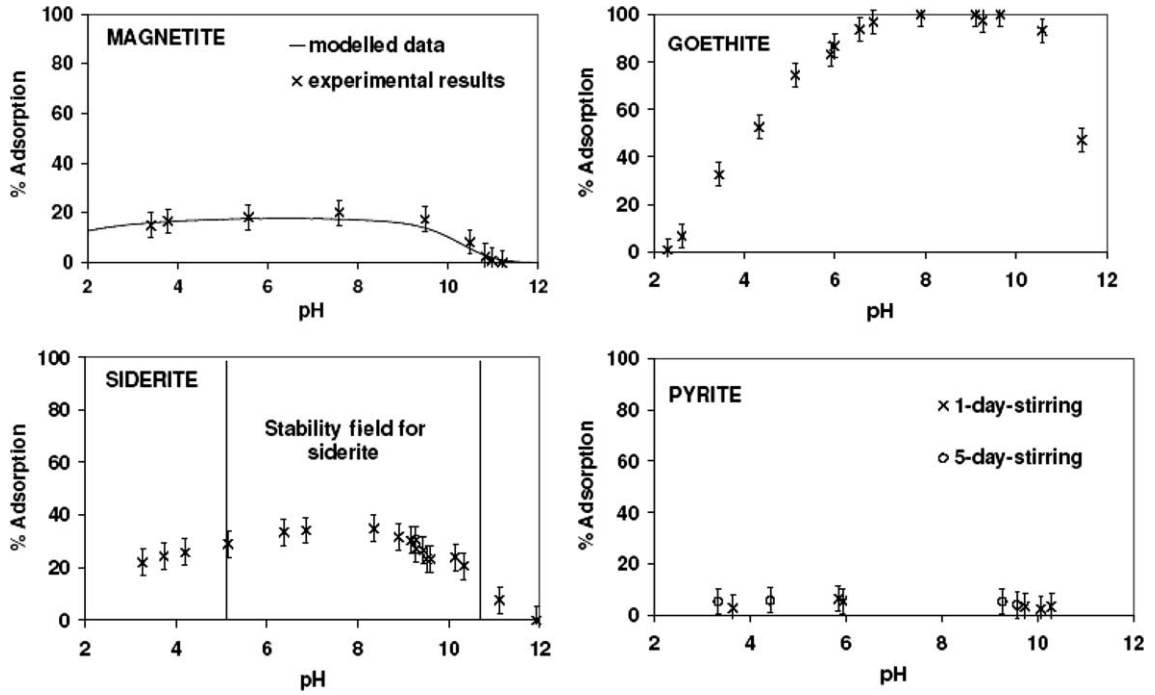

Fig. 2. (magnetite) Sorption of Si (4.72×10^{-5} mol L^{-1}) on magnetite (2 g L^{-1}) in NaCl (0.1 mol L^{-1}). Crosses represent the experimental data and the line shows FITEQL calculations. (goethite) Sorption of Si (1×10^{-4} mol L^{-1}) on goethite (10 g L^{-1}) in NaCl (0.1 mol L^{-1}). (siderite) Sorption of Si (5.54×10^{-5} mol L^{-1}) on siderite (2 g L^{-1}) in NaCl (0.1 mol L^{-1}). The stability field of siderite was determined from the thermodynamic data of Table 6. (pyrite) Sorption of Si (1×10^{-4} mol L^{-1}) on pyrite (8 g L^{-1}) in $NaClO_4$ (0.05 mol L^{-1}).

Saturation curve for suspension of 2 g L^{-1} in 0.1 mol L^{-1} sodium chloride with various concentrations in silicon (ranging from 10 to 300 μmol L^{-1}) at pH 9.5, leads to a sorption capacity of 79 ±21 $\mu mol_{Si}\ g^{-1}_{goethite}$ (Fig. 3).

4.2.3. Siderite

Fig. 2 shows the effects of pH on the amount of Si sorbed (5.54×10^{-5} mol L^{-1} solution) on siderite (2 g L^{-1}) in 0.1 mol L^{-1} NaCl electrolyte. The first part of the graph presents a gradual growth from 30% at pH 3.3 up to 48% at pH 6.4. Then sorption remains constant at the same level from pH 6.4 to pH 8.4. The third portion reveals a rapid decline from 48% at pH 8.4 down to 0% at pH 12. So, sorption curve leads to a maximal sorption onto magnetite surface from pH 6.4 to pH 8.4, i.e. in its field of stability. Due to the fact that siderite is only stable between pH 5.5 and pH 10.5, the results for more acidic or basic pH are not representative of siderite sorption.

Saturation curve for suspension of different siderite concentrations (from 4 to 8 g L^{-1}) in 0.1 mol L^{-1} sodium chloride with various concentrations in silicon (ranging from 25 to 500 μmol L^{-1}) at pH 8.5, leads to a sorption capacity of 20 ± 8 $\mu mol_{Si}\ g^{-1}_{siderite}$ (Fig. 3).

4.2.4. Pyrite

Fig. 2 shows the effects of pH on the amount of Si sorbed (3.56×10^{-5} mol L^{-1} solution) on pyrite (8 g L^{-1}) in 0.05 mol L^{-1} $NaClO_4$ electrolyte. The percentage of adsorption remains quite stable (from 3% to 6%) for all pH and is not significative. No saturation experiment was therefore carried out.

4.2.5. Interpretation

Sorption of cations or neutral species often steadily increases with pH in acidic conditions [9,11,18–20] whereas sorption of anions is often associated with a sharp decrease with pH in alkaline conditions [21,22]. These behaviors are typical of sorption of cations and anions on oxi-hydroxides. Cationic species can sorb on negative deprotonated surface sites ($\equiv XO^-$). Conversely, anionic species sorb on positive protonated surface sites ($\equiv XOH_2^+$). In this study, three-part curves were observed for silicon sorption on magnetite, goethite and siderite, which can be explained as follows:

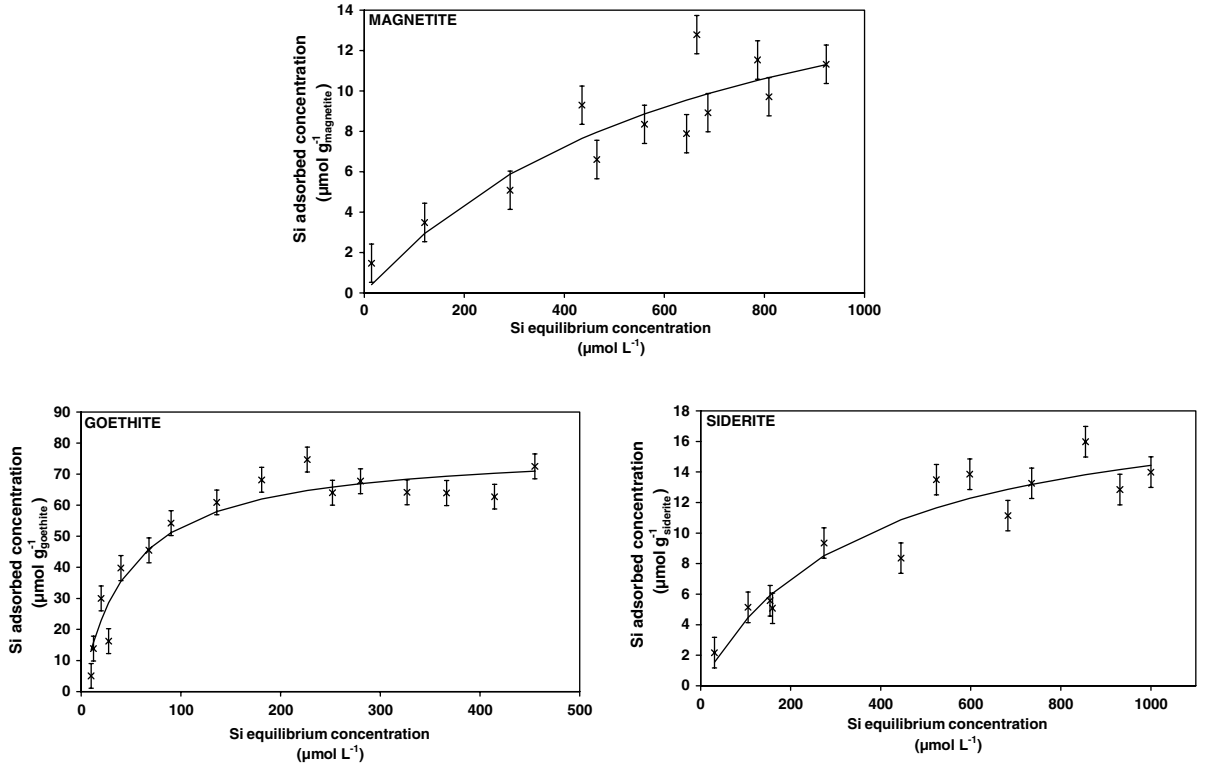

Fig. 3. (magnetite) Saturation of magnetite (at different concentrations) at pH 8.5 in NaCl (0.1 mol L^{-1}). (goethite) Saturation of goethite (2 g L^{-1}) at pH 9.5 in NaCl (0.1 mol L^{-1}). (siderite) Saturation of siderite (at different concentrations) at pH 8.5 in NaCl (0.1 mol L^{-1}).

- The first part, i.e. the increase of Si sorption with pH, can be explained by Eq. (9) the release of H^+ associated with Si sorption:

$$\equiv XOH_2^+ + H_4SiO_4 \rightleftharpoons \equiv X(OH_2)Si(OH)_3 + H^+. \quad (9)$$

  Note that eliminating H_2O in $\equiv X(OH_2)Si(OH)_3$ gives $\equiv XOSi(OH)_3$, and leads to the same pH dependency. The difference between the two Si sorbed species is that silicon is in the second surface layer in the former while $\equiv XOSi(OH)_3$ is a surface complex directly coordinated on the surface in the latter.
- For the second part, i.e. the plateau, three assumptions can be put forward:
  (1) sorption sites on corrosion product surface could be saturated,
  (2) all the silicon species introduced in the batch could be sorbed,
  (3) sorption of other anionic species, typically OH^-, could be in competition with $H_3SiO_4^-$. The resulting reaction:

$$\equiv XOH + H_4SiO_4 \rightleftharpoons \equiv X(OH_2)Si(OH)_3 \quad (10)$$

  does not depend on pH (Eq. (10)). The first hypothesis seemed to be the most relevant when the results of sorption and saturation experiments are compared. Nonetheless, there is an important uncertainty on the saturation data. It is due to the fact that when there is only a small amount of corrosion product in the batch, namely 50 or 100 mg, bigger quantity of silicon is uptaken. Indeed, the experimental points above the fitted curves are obtained in batch containing small amounts of corrosion products.
- The last part, i.e. the decrease of Si sorption with pH, can be explained by the deprotonation of aqueous H_4SiO_4 at pH more than 9.

$$\equiv XOH + H_3SiO_4^- + H^+ \rightleftharpoons \equiv X(OH_2)Si(OH)_3. \quad (11)$$

  The sorption of Si is associated with an H^+ uptake.

Reasonable interpretations are consistent with the observed trends but this is not enough to

establish sorption mechanisms, so that modelling was used (see Section 4.3).

4.3. Modelling Si sorption on magnetite

All the parameters we need for the modelling (surface area, sorption site density and acidity constants) were experimentally determined. So the only additional fitting parameters are the surface complexation constant(s) and the stoichiometry of the sorbed Si species. Experimental data were modelled with monodentate and bidentate complexes since ratios 4:1 to 1:1 were observed between the proton sites concentration and the sorbed Si concentration at saturation at pH 8.5, taking the uncertainty into account (Table 3). Nevertheless, with the monodentate complex, the modelled curve quite poorly fitted the experimental results, while the fit is better when using the complexation reaction:

$$2 \equiv \mathrm{XOH} + \mathrm{H_4SiO_4} \rightleftharpoons (\equiv \mathrm{XO})_2\mathrm{Si(OH)_2} + 2\mathrm{H_2O}. \quad (12)$$

The parameters used to fit the experimental curve and the surface complexation constant calculated by FITEQL ($\log K_{\mathrm{complexation}} = 8.6$) are summarized in Table 4 and the experimental and the fitted curves are represented in Fig. 2. There is a good agreement between the experimental and the modelled data.

The silicon aqueous speciation was then calculated taking the so defined surface complex into account (Fig. 4). Silicon speciation is quite similar with or without silicon sorption, due to the relative small amount of sorbed silicon on magnetite (Tables 5 and 6).

4.4. Modelling glass alteration

From data obtained during saturation experiments, we can estimate an upper limit for the increase of nuclear glass alteration due to Si uptake by the corrosion products. Alteration was modelled

Table 4
Modelling parameters

	Magnetite
$\log K_{a1}$	−3.87
$\log K_{a2}$	−8.89
Specific surface area ($m^2\ g^{-1}$)	1.8
[SiO_2] (mol L^{-1})	4.7×10^{-5}
[magnetite] (g L^{-1})	2
[X–OH] (mol L^{-1})	4×10^{-5}
$\log K_{\mathrm{complexation}}$	8.6

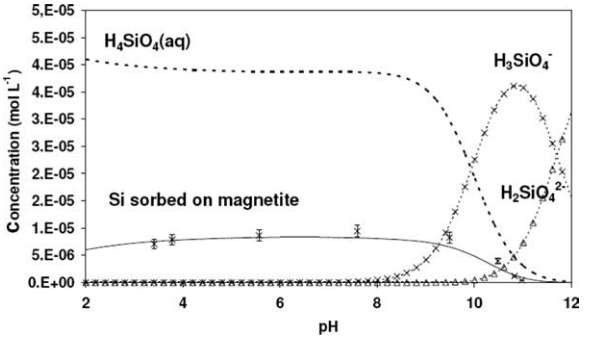

Fig. 4. Speciation curve of silicon (4.72×10^{-5} mol L^{-1}) after sorption on magnetite (2 g L^{-1}) in NaCl (0.1 mol L^{-1}).

Table 5
Silicon speciation modelling parameters

Equilibria	$\log K$ (25 °C)
$H_4SiO_4 \rightleftharpoons H_3SiO_4^- + H^+$	−9.93
$H_4SiO_4 \rightleftharpoons H_2SiO_4^{2-} + 2H^+$	−21.62
Quartz solubility	1×10^{-4} mol L^{-1}

Table 6
Siderite stability modelling parameters

Equilibria	$\log K$ (25 °C)
$Fe^{2+} + HCO3^- \rightleftharpoons FeCO_3 + H^+$	0.19
$Fe^{2+} + HCO3^- \rightleftharpoons FeHCO_3^+$	2.72
$Fe^{2+} + H_2O \rightleftharpoons FeO + 2H^+$	−13.53
CO_2 (aq) + $H_2O \rightleftharpoons H_2CO_3$	−1.46
$HCO_3^- \rightleftharpoons CO_3^{2-} + H^+$	−10.33
$H_2CO_3 \rightleftharpoons HCO_3^- + H^+$	−6.40

Table 3
Percentage of proton sites saturated with silicon species

	Total proton sites (mol g^{-1})	Silicon retained ($mol_{Si}\ g^{-1}$)	$\frac{\text{Silicon retained}}{\text{Total proton sites}}$ (%)
Magnetite	20×10^{-6}	$19 \pm 14 \times 10^{-6}$	25–100
Goethite	57×10^{-6}	$79 \pm 21 \times 10^{-6}$	100
Siderite	Not determined	$20 \pm 8 \times 10^{-6}$	Not determined

with magnetite. Firstly, the maximum mass of synthesized magnetite ($m_{\text{magnetite}}$) and those of sorbed silicon ($m_{\text{Si sorbed}}$) were calculated, considering 2144 kg of iron (m_{Fe}) for the canister, the overpack and the casing each would be completely oxidised.

$$m_{\text{magnetite}} = m_{\text{Fe}} \times \frac{M_{\text{magnetite}}}{M_{\text{Fe}}} = 8.89 \text{ kg}, \quad (13)$$

$$m_{\text{Si sorbed}} = \text{sorption capacity}_{\text{magnetite}} \times m_{\text{magnetite}} \times M_{\text{Si}} = 4.74 \text{ kg}, \quad (14)$$

where m_i and M_i are the mass and the molecular mass of i, respectively.

The glass frit used to contain radioactive waste is a borosilicate glass which consists mainly of SiO_2 (about 45 wt%). Each canister is initially filled with 400 kg (m_{canister}) of the borosilicate glass namely 84 kg of silicon ($m_{\text{Si in a canister}}$). The durability of containment is controlled by the glass alteration kinetics. The mass of solubilized glass ($m_{\text{solubilized glass}}$) can be calculated as follows:

$$m_{\text{solubilized glass}} = m_{\text{Si sorbed}} \times \frac{m_{\text{canister}}}{m_{\text{Si in a canister}}} = 22.59 \text{ kg}. \quad (15)$$

The geometric surface of glass package is 1.7 m^2 and nuclear glass density is 2800 kg m^{-3} (ρ_{glass}), so the alterated glass thickness would be:

$$\text{total alteration thickness} = \frac{m_{\text{solubilized glass}}}{\text{geometric surface} \times \rho_{\text{glass}}} = 4.74 \times 10^{-3} \text{ m}, \quad (16)$$

which is quite small. The annual alterated glass thickness is the ratio of the initial glass dissolution rate ($r_o = 0.01$ g m^{-2} J^{-1} corresponding to 3.65×10^{-3} kg m^{-2} $year^{-1}$ at 50 °C) on glass density [23], it would be

$$\text{annual alteration thickness} = \frac{r_0}{\rho_{\text{glass}}} = 1.30 \times 10^{-6} \text{ m year}^{-1}. \quad (17)$$

The ratio of the total alterated glass thickness on the annual alterated glass thickness leads to the period of time (t) during which glass would be altered at its initial rate.

$$t = \frac{\text{total alteration thickness}}{\text{annual alteration thickness}} = 3650 \text{ years}, \quad (18)$$

which is small compared with the glass expected lifetime (300 000 years). Silicon sorption onto corrosion products would only have a small influence on glass alteration.

5. Conclusion

Sorption of silicon on various corrosion products of iron was studied. The physico-chemical properties (microstructure, surface area and surface charge) of the solids were analyzed in detail before the sorption experiments. The effect of equilibrium pH on the amount of silicon sorbed on corrosion product surface was studied. The maximum pH of sorption corresponds to the expected pH during glass leaching in underground conditions (pH 8.5). Saturation experiments were carried out at the pH corresponding to the maximum sorption. Saturation curves were fitted with the Langmuir equation. Only three of the four studied corrosion products are able to sorb silicon, but in different proportions: $(19 \pm 14) \times 10^{-6}$ mol_{Si} $g^{-1}_{magnetite}$, $(79 \pm 21) \times 10^{-6}$ mol_{Si} $g^{-1}_{goethite}$ and $(20 \pm 8) \times 10^{-6}$ mol_{Si} $g^{-1}_{siderite}$. Pyrite surface has no affinity for silicon dissolved species. The saturation data obtained during experiments enabled us to model glass alteration in presence of corrosion products. Sorption capacity of magnetite would only have a small influence on glass alteration since glass would be altered at its initial rate during up to 3650 years i.e. 1.2% of its total lifetime.

In the future, research should consider ankerite ($FeCa(CO_3)_2$) because it is ubiquitous in soils. Moreover, the temperature influence must be evaluated since in the deep disposal, the waste package will reach, at least, 50 °C.

Acknowledgement

The authors thank Dr Pierre Vitorge from the Commissariat à l'Energie Atomique for the fruitful discussions regarding the theoretical interpretation of experimental data.

References

[1] C. Bataillon, C. Musy, M. Roy, J. Phys. IV France 11 (2001) 267.
[2] J.M. Gras, C.R. Physique 3 (2002) 891.
[3] D. Neff, S. Reuger, L. Bellot-Gurlet, P. Dillmann, R. Bertholon, J. Raman Spectrosc. 35 (2004) 739.
[4] D. Neff, S. Reuger, L. Bellot-Gurlet, G. Beranger, Corros. Sci. 47 (2005) 515.
[5] E. Vernaz, C.R. Physique 3 (2002) 813.

[6] P. Jollivet, Y. Minet, M. Nicolas, E. Vernaz, J. Nucl. Mater. 281 (2000) 231.
[7] J.C. Westall, A. Herbelin, FITEQL v 3.2: A computer program for the determination of equilibrium constants from experimental data, Department of Chemistry, Oregon State University, Corvallis, 1996.
[8] J. Van der Lee, L. de Windt, CHESS Tutorial and Cookbook, Technical Report LHM/RD/99/05, Ecole des Mines de Paris, Fontainebleau, 1999.
[9] H. Catalette, J. Dumonceau, P. Ollar, J. Contam. Hydrol. 35 (1998) 151.
[10] H. Catalette, Sorption de cations d'intérêt nucléaire à la surface de produits de corrosion, PhD. Thesis, Orsay University, France, in press.
[11] A. Naveau, F. Monteil-Rivera, J. Dumonceau, S. Boudesocque, J. Contam. Hydrol. 77 (2005) 1.
[12] D.A. Dzomback, F.M.M. Morel, Surface Complexation Modeling: Hydrous Ferric Oxide, Wiley-InterScience, New York, 1990.
[13] W.A. Kornicker, J.W. Morse, Geochim. Cosmochim. Acta 55 (1991) 2159.
[14] L. Charlet, P. Wersin, W. Stumm, Geochim. Cosmochim. Acta 54 (1990) 2329.
[15] P. van Cappellen, L. Charlet, W. Stumm, P. Wersin, Geochim. Cosmochim. Acta 57 (1993) 3505.
[16] N. Marmier, J. Dumonceau, J. Chupeau, F. Fromage, C. R. Acad. Sci., Ser. 2 317 (1993) 1561.
[17] M. Descostes, P. Vitorge, C. Beaucaire, Geochim. Cosmochim. Acta 68 (2004) 4559.
[18] T. Missana, M. Garcìa-Gutiérrez, C. Maffiotte, J. Colloid Interface Sci. 260 (2003) 291.
[19] R.S. Juang, J.Y. Chung, J. Colloid Interface Sci. 275 (2004) 53.
[20] T. Missana, M. Garcìa-Gutiérrez, V. Fernǹdez, Geochim. Cosmochim. Acta 67 (2003) 2543.
[21] J.M. Zachara, P.L. Gassman, C.S. Smith, D. Taylor, Geochim. Cosmochim. Acta 59 (1995) 4449.
[22] M. Duc, G. Lefevre, M. Fedoroff, J. Janine, J.C. Rouchaud, F. Monteil-Rivera, J. Dumonceau, S. Milonjic, J. Environ. Radioact. 70 (2003) 61.
[23] E. Vernaz, S. Gin, C. Jégou, I. Ribet, J. Nucl. Mater. 298 (2002) 27.